PROCEEDINGS OF THE SEVENTEENTH LUNAR AND PLANETARY SCIENCE CONFERENCE, PART 2
JOURNAL OF GEOPHYSICAL RESEARCH, VOL. 92, NO. B4, PAGES E575–E587, MARCH 30, 1987

On The Spectral Reflectance Properties of Materials Exposed at the Viking Landing Sites

EDWARD A. GUINNESS, RAYMOND E. ARVIDSON, MARY A. DALE-BANNISTER

McDonnell Center for the Space Sciences, Department of Earth and Planetary Sciences, Washington University, St. Louis, Missouri

ROBERT B. SINGER AND EILEEN A. BRUCKENTHAL

Planetary Geosciences Division, Hawaii Institute of Geophysics, University of Hawaii, Honolulu

Bidirectional reflectances, calibrated to within 10% uncertainties, for blue (0.40–0.52 μm), green (0.50–0.59 μm), and red (0.60–0.74 μm) channels were determined for 31 block and soil exposures imaged by the Viking Lander Cameras. Reflectances were corrected for atmospheric attenuation by using optical depth measurements obtained by the Lander Cameras and for skylight illumination by subtracting the brightness values of adjacent shadowed areas. Reflectances for two facets on each of two large blocks were computed for a common geometry by determining facet orientations from high resolution Lander stereo images and by fitting the Hapke-Irvine photometric function to reflectances estimated for several geometries. Results indicate that individual facets on the same block have different optical properties. The darkest, grayest block facets have properties similar to laboratory reflectance spectra of mafic rocks that are thinly coated with ferric iron-rich palagonite. Most block surfaces have reflectances consistent with thin to optically thick covers of palagonitic material. Limited exposures of soil have spectra that are also similar to palagonitic material. The majority of the soils sampled and a few block surfaces have spectra with steeper slopes and greater spectral curvatures than the palagonite analog, consistent with greater degree of ferric iron crystallinity. The soils could be an intimate mixture of palagonitic material and other materials not seen in end member form, but, if so, these other materials would need an even greater slope and curvature than observed soils. The differences in reflectance properties for common block surfaces compared to common soils imply that local weathering of blocks has not contributed significantly to the soil exposed at the landing sites.

INTRODUCTION

Two identical imaging systems were included on each of the Viking Landers that touched down on Mars in 1976. The cameras produced monochrome, high resolution (0.04° angular resolution) images of the surface, where features as small as a few centimeters across could be distinguished in the near field [*Binder et al.*, 1977; *Mutch et al.*, 1977]. Multispectral data were also acquired in six broad wavelength bands covering the 0.4 to 1.1 μm region with an angular resolution of 0.12° [*Huck et al.*, 1977]. In a number of research efforts the six-channel data were used to constrain the variety and types of soils and blocks exposed at the landing sites [*Huck et al.*, 1977; *Strickland*, 1979; *Evans and Adams*, 1979, 1980; *Guinness*, 1981; *Singer and Strickland*, 1981; *Arvidson et al.*, 1983]. These studies indicated that there are variations in soil and block colors, although it was not known whether the variations were due to mineralogical differences, to lighting and viewing geometry differences, or to particle size effects [*Huck et al.*, 1977; *Guinness*, 1981]. Some blocks at each site are less red than the soil, which suggests that they are less weathered, whereas other blocks appear to be brighter and redder than soils [*Strickland*, 1979]. In addition, previous comparisons of Lander multispectral data with laboratory spectral reflectance data suggest similarities to samples of weathered basaltic tephra [*Evans and Adams*, 1979, 1980].

Despite past efforts, there has yet to be a comprehensive examination of the multispectral data that combines testing of the camera radiometric calibrations, explicitly removing the effects of atmospheric attenuation and skylight, correcting soil and block reflectance estimates to values of common lighting and viewing geometries, and quantitatively comparing the corrected data to reflectance estimates from analog materials. This paper and the recent work of *Adams et al.* [1986] report such comprehensive efforts. The goal of this paper is to characterize the types of soils and blocks exposed, and to search for evidence of relatively unaltered igneous materials.

Paper number 6B7221.
0148-0227/87/006B-7221$05.00

RADIOMETRIC CALIBRATION OF THE VIKING LANDER CAMERAS

Crucial to analyses of reflectance estimates from Lander Camera data is a rigorous consideration of radiometric calibrations, so that uncertainties in the derived reflectance estimates will be known. A description of the Viking Lander Cameras and their performance during the early portion of the mission is given by *Patterson et al.* [1977]. The components of the imaging system and the integrated system were initially calibrated through a series of preflight experiments where targets of known radiometric properties were illuminated by a calibrated light source [*Huck et al.*, 1975].

During flight to Mars and during the time the Landers were operational on the surface, relative calibrations were acquired by imaging an internal light source. Sterilization of the Landers to meet Mars quarantine requirements, together with neutron radiation from radioisotope thermoelectric generators on the Landers, could have caused changes in calibrations relative to preflight conditions. More importantly, both the heat and the neutrons could have affected the wavelength dependence of the channel responsivities, although direct evidence for these changes is lacking. These effects should be greatest for the three infrared channels [*Patterson et al.*, 1977]. Thus it is important to carefully consider the calibration of each of the six multispectral channels, preferably using a method that independently provides corrections to preflight values.

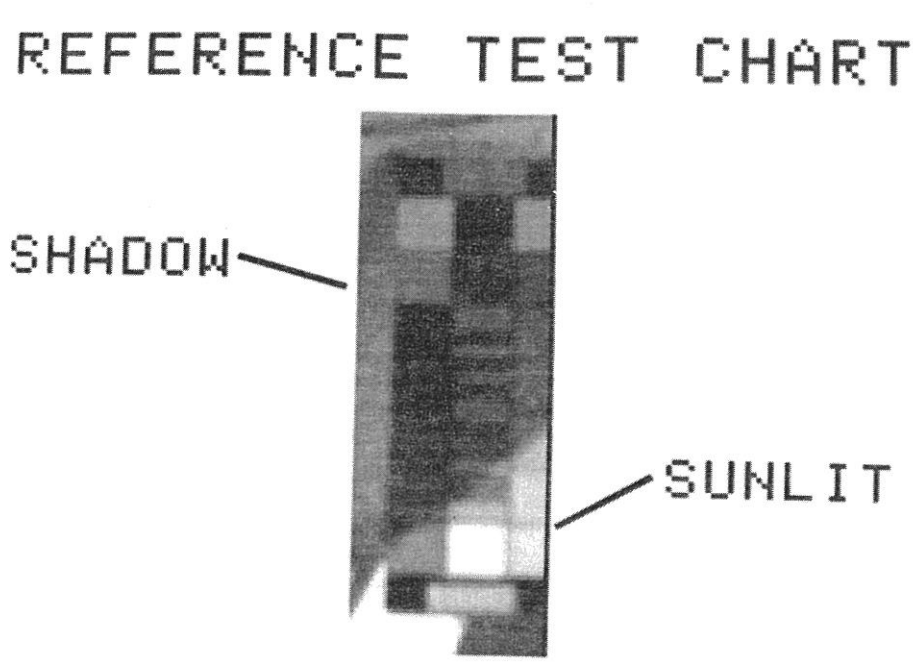

Fig. 1. Viking Lander red channel image 21A099 (Lander 2, Camera 1, frame A099) showing a partially shadowed RTC. Voltage data derived from this image are plotted in Figure 2.

Huck et al. [1977] calibrated the Lander imaging data by normalizing preamplifier voltage values received from soils and blocks to voltage values from a series of gray patches [known as Reference Test Charts (RTC)] mounted on the Landers. However, the RTCs are located on top of the Lander decks, where differences in illumination between the deck and the surface may introduce complications. Thus we chose to evaluate the preflight calibrations directly using Lander images of RTCs in an experiment where we explicitly remove indirect illumination effects and compensate for atmospheric attenuation. The voltage (V_j) received from the jth (j = 1 to 6) multispectral channel for one of the RTC gray patches can be modeled as [*Huck et al.*, 1977; *Guinness*, 1981]

$$V_j = K_j \rho \cos i \int I_o(\lambda) \exp[-\tau/\mu_o] R_j(\lambda)\, d\lambda + K_j \rho_H \int E_s(\lambda) R_j(\lambda)\, d\lambda \quad (1)$$

The first term on the right is due to the direct solar beam: K_j is the preflight calibration constant of the jth channel, ρ is the bidirectional reflectance of a gray patch, i is the local solar incidence angle of the RTC, $I_o(\lambda)$ is the solar spectral irradiance, τ the atmospheric optical depth, μ_o the cosine of the solar incidence angle relative to the zenith, and $R_j(\lambda)$ is the jth channel spectral responsivity. The second term is due to skylight and any light reflected from the Lander: The spectral irradiance due to the combination of these sources is $E_s(\lambda)$ and the hemispherical reflectance of a gray patch is ρ_H. Preflight estimates of K_j and $R_j(\lambda)$ can be found in *Huck et al.* [1975] for each of the four camera systems (two per Lander).

Atmospheric optical depths (τ) were determined frequently during the beginning of the Lander missions by imaging the sun at two elevation angles with a broad-band photodiode specially configured for that purpose [*Pollack et al.*, 1977]. Beer's Law was then used to compute optical depth without the need for absolute calibrations. Optical depth measurements are accurate to about ±0.1 and, to a good approximation, are independent of wavelength for the region of 0.4 to 1.0 μm [*Pollack et al.*, 1977]. Optical depths varied from approximately 0.3 during the beginning of the mission to values in excess of 8.0 during dust storms [*Pollack et al.*, 1979]. Even with an optical depth of 0.3, skylight is an important illumination source. For example, with an incidence angle as low as 10 degrees, the solar irradiance will be about 74% of its extra-atmospheric value. The remaining 26% is absorbed or scattered, with some fraction of the scattered light diffusely illuminating the scene as skylight. Thus the skylight term must be dealt with in testing calibration of Lander data or in quantitative analyses of the soil or block data.

As a means of directly evaluating skylight, we examined color images of partially shadowed RTCs for both cameras on each Lander (Figure 1). We chose RTCs that were mounted above the Lander deck and that were free from dust coatings [*Guinness et al.*, 1979]. An RTC contains 11 gray patches, each with a different absolute reflectance, and each being a Lambertian scatterer [*Wall et al.*, 1975]. Figure 2 is a plot of preamplifier voltage for the red channel versus gray patch bidirectional reflectance for gray patches seen by Camera 1 on Lander 2. The two lines correspond to linear least-squares fits to data for shadowed and sunlit patches. The voltage received from the shadowed patches is equal to the second term on the right side of (1) (i.e., the skylight component). The slope of the fit to the shadowed patch data is therefore equal to the integral of the indirect illumination term multiplied by the calibration constant. Thus the observed voltage of a sunlit patch can be corrected for indirect illumination by subtracting a voltage computed by multiplying the reflectance of the sunlit patch by the slope of the fit to the shadowed patch data.

The voltage corrected in this manner for a given multispectral channel is equal to

$$V_c = \exp[-\tau/\mu_o] \rho \cos i\, K \int I_o(\lambda) R(\lambda)\, d\lambda \quad (2)$$

where V_c is the corrected voltage of a sunlit patch. For a given RTC image, (2) has the form of voltage equal to a constant times the patch reflectance, where the constant (M) is the

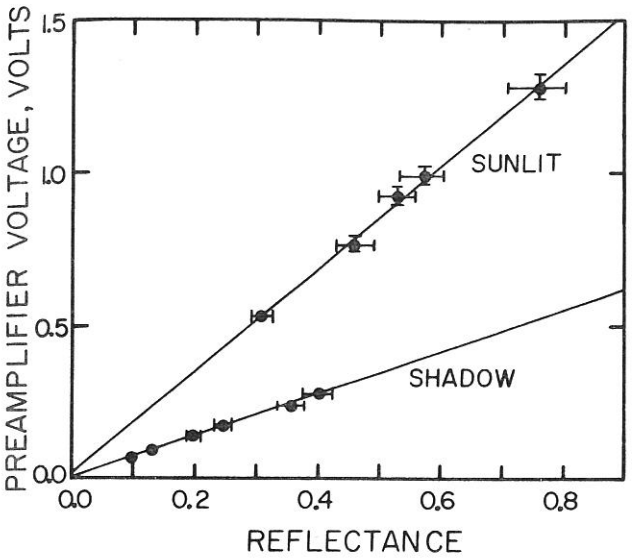

Fig. 2. This is a plot of voltage versus RTC patch reflectances for sunlit and shadowed gray patches from the RTC seen in Figure 1. Data for the red channel are shown. The relative error in voltage is 3% [*Huck et al.*, 1975] and the error in gray patch reflectance is 6% [*Wall et al.*, 1975]. The solid lines are for linear least-squares fits to the data.

following

$$M = \exp[-\tau/\mu_o] \cos i \, K \int I_o(\lambda) \, R(\lambda) \, d\lambda \quad (3)$$

M can be estimated from a least-squares fit to the corrected voltage data of sunlit patches. A value for the term on the right side of (3) can also be computed using preflight values for K and R, values of μ_o and i determined from the lighting geometry, and an estimate for τ. The values of τ are uncertain, partially because optical depth measurements were not made at the same time as the RTC images were acquired. An optical depth value, which was measured close in time (within a few Mars days) to a given RTC image, was used to compute values of M. For the color images, observed M values differed from computed values by about 6% for Camera 1 on Lander 1, 35% for Camera 2 on Lander 1, 11% for Camera 1 on Lander 2, and 14% for Camera 2 on Lander 2. Except for Camera 2 on Lander 1, these results are consistent with the combined 8% uncertainty for the radiometric calibrations measured in the preflight tests [*Patterson et al.*, 1977], 3% uncertainty in the analog-to-digital conversion [*Huck et al.*, 1975], and the uncertainty in the optical depth value. Thus we conclude that the preflight calibrations for the color channels are still valid (with the possible exception of Camera 2 on Lander 1) and that reflectances can be computed with an uncertainty of about ±10% due to radiometric calibration and analog-to-digital conversion uncertainties.

Partially shadowed RTC images acquired with the three infrared channels are only available for Camera 1 on Lander 1. Computed gray patch voltages for the three infrared channels (0.81–1.07 μm) are a factor of 2 to 3 higher than measured values. This result suggests that there have been changes in the calibration constants of the infrared channels or wavelength dependent changes in the spectral responsivity functions. Both types of changes are predicted from modeling of neutron induced degradation of the infrared channels [*Patterson et al.*, 1977]. Thus the infrared channels are poor prospects for extraction of absolute reflectance. More importantly, it is difficult to make comparisons with laboratory samples since we can not determine the nature of the wavelength dependent changes to the responsivity functions. As a result, we limit our analysis of absolute reflectances to data from the blue (0.40–0.52 μm), green (0.50–0.59 μm), and red (0.60–0.74 μm) channels from the three cameras where the preflight calibration data are still valid. Although not shown, it is clear from the RTC data that voltage versus RTC gray patch reflectance is still linear for the infrared channels. This suggests that the IR channel detector sensitivities are still linear, although absolute values and IR spectral properties are questionable. Thus the infrared channels were used to explore relative brightness variations with wavelength, albeit in more qualitative ways than with the blue, green, and red channels.

Extraction of Soil and Block Spectral Reflectance Values

In this section we discuss the method for computing reflectances from Lander images. The shapes of the Lander Camera spectral responsivity functions are sufficiently irregular that assigning center wavelengths to the channels can be misleading [*Huck et al.*, 1977]. Thus the analyses are restricted to quoting bidirectional reflectance estimates for the blue, green, and red channels. The approach we used is derived from *Guinness* [1981]. As in the analysis of RTC images, we treat the total illumination as the sum of direct and skylight components. The skylight contribution to the voltage received from a given sunlit sample of soil or block was estimated by subtracting the voltage received from a nearby shadow on the same soil or block exposure. Such an estimate of the skylight component is reasonable, even if the sunlit and shadowed samples have slightly different spectral properties, because the brightness of shadows varies very little throughout an image. An atmospheric optical depth value, measured closest in time to when the surface data were acquired, was then used, along with the solar irradiance [$I_0(\lambda)$] at the Mars-Sun distance (which was 1.65 AU and 1.61 AU for the images used in our analysis), preflight calibration constants [K_j], and spectral responsivity data [$R_j(\lambda)$], to compute the bidirectional reflectance relative to a Lambertian surface of unit reflectance

$$\rho_j = \frac{[V_{j,SUN} - V_{j,SHADOW}]}{\exp[-\tau/\mu_o] \, K_j \int I_o(\lambda) \, R_j(\lambda) \, d\lambda} \quad (4)$$

where j refers to the jth channel. The quantity, ρ_j, represents the weighted average bidirectional reflectance over the wavelength range of the jth channel. Bidirectional spectral reflectance estimates were computed for 31 samples of soils and blocks. For reference, the locations of these samples are shown in Figure 3. Blue, green, and red reflectance values for the soils and blocks samples are summarized in Table 1. Table 1 also lists the phase angles that pertain to each reflectance measurement.

Photometric Properties of Selected Blocks

A number of authors [*Strickland*, 1979; *Evans and Adams*, 1979; *Sharp and Malin*, 1984; *Adams et al.*, 1986] have noted variations in color and albedo between different portions of

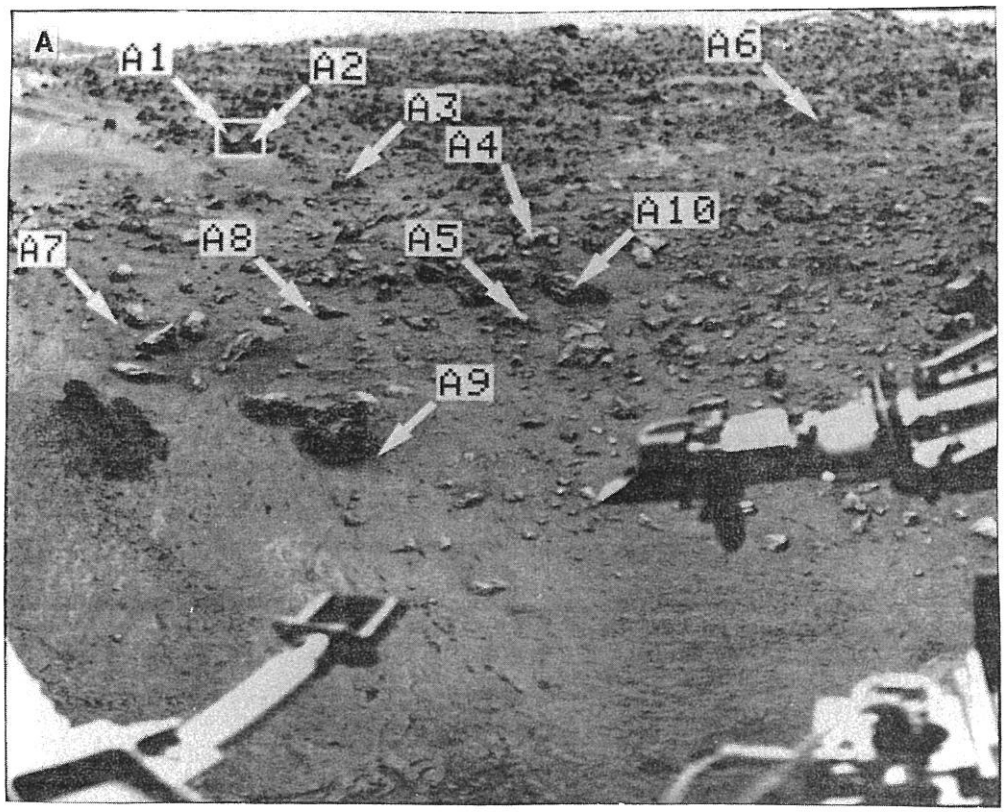

Fig. 3*a*

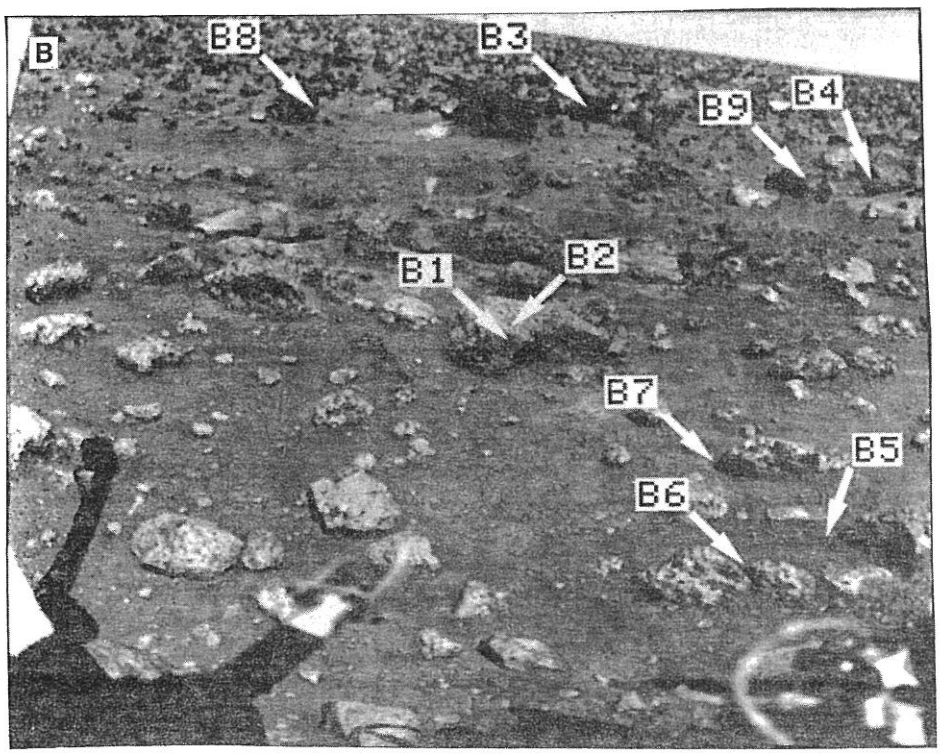

Fig. 3*b*

Fig. 3. Images acquired by the red channel covering a portion each Viking Lander site. Arrows point to soils and blocks for which reflectance estimates were obtained. The sample numbers are referred to in Table 1. Boxes outline blocks investigated in detail and shown in Figures 4 and 5. (*a*) VL1 image 11A147. (*b*) VL2 image 21A187. (*c*) VL2 image 22A190.

Lander blocks. The variations can be interpreted in terms of a variable extent of coating of blocks by fine-grained ferric iron-rich weathering materials or in terms of variable mixtures of weathered soil and relatively unweathered rock components [*Adams et al.*, 1986]. On the other hand, the differences might be apparent and only due to variations in local incidence and emission angles. To test for homogeneity in spectral properties of given blocks, we considered in detail the local geometry and

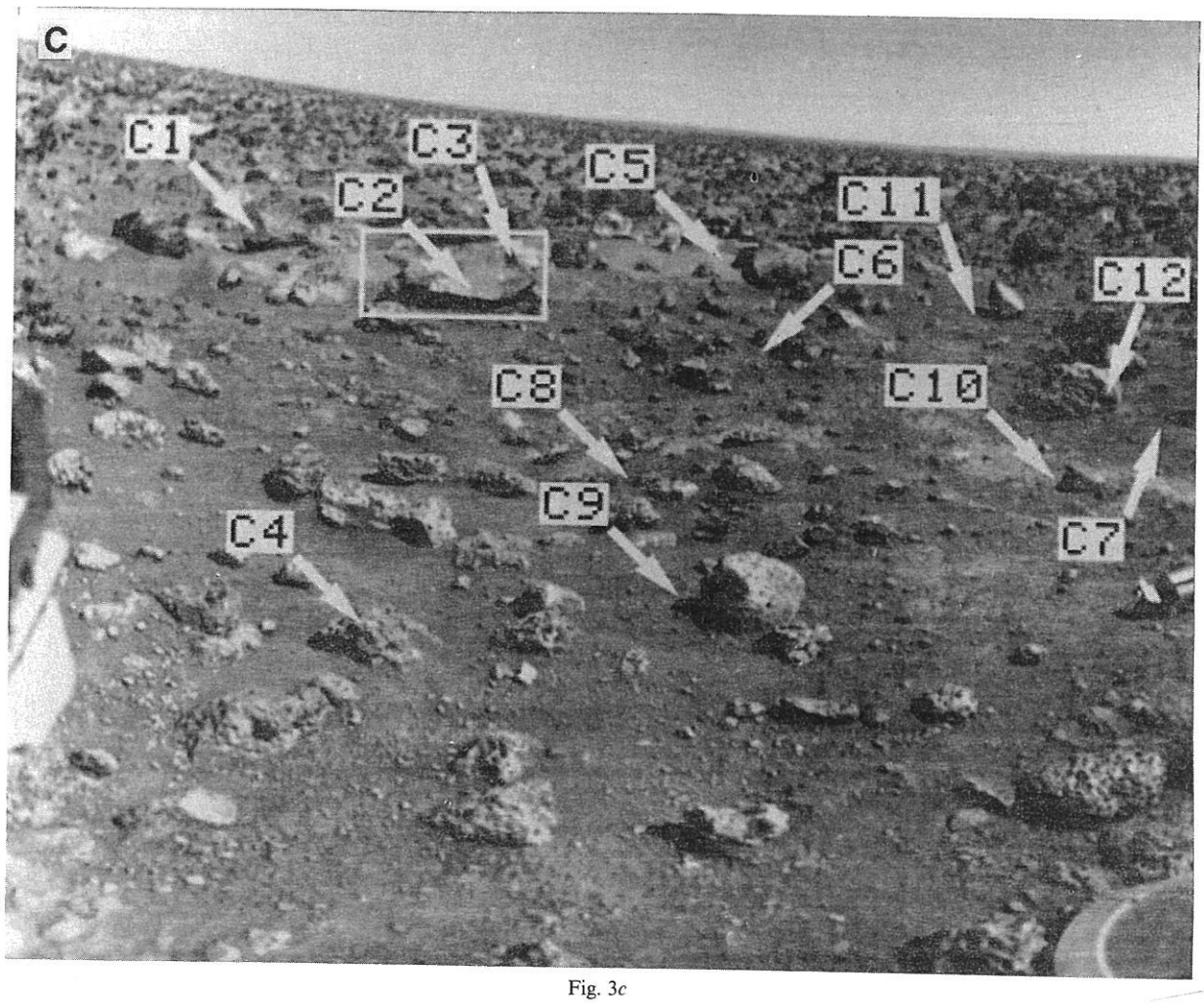

Fig. 3c

Fig. 3. *(continued)*

reflectance properties of two relatively large, angular blocks, hereby named VL1 and VL2 blocks. They are shown in the areas enclosed by boxes in Figure 3 and in high resolution images in Figures 4 and 5. Blue, green, and red bidirectional reflectances for selected facets on these blocks determined at a variety of incidence, emission, and phase angles were fit to the Hapke-Irvine photometric function. This function has the following form

$$\rho = 2\ B_o\left[\frac{\mu_o}{\mu_o+\mu}\right]\ \exp\left[\alpha\ g\right] \qquad (5)$$

where: B_0, α are independent variables influenced by material properties; μ_0, μ are the cosines of the incidence and emission angles, respectively, and g is the phase angle. A more complicated photometric function by *Hapke* [1981], which accounts for the opposition effect at small phases, has been shown to fit photometric data for soil at the Viking 1 site [*Guinness*, 1981]. We choose to use the simpler Hapke-Irvine function because of its applicability to a wide range of materials [see *Gradie et al.*, 1980] and because the data available for the blocks were acquired at relatively large phase angles, where the opposition effect is insignificant. Equation 5 can be rewritten as

$$\log\left[\frac{\rho\ (\mu_o+\mu)}{(2\ \mu_o)}\right] = \log B_o + \alpha\ g \qquad (6)$$

Values of B_0 and α were estimated from linear least-squares fit to the data with the term on the left side of (6) as the dependent variable and phase angle as the independent variable. The estimated values of B_o and α were used in (5) to compute reflectances for all facets at a common geometry.

Reflectance data for two facets on VL1 block were obtained at various incidence and phase angles from a series of four images acquired on a single Mars day. Stereo ranging from high spatial resolution images from the two Lander Cameras [see *Liebes and Schwartz*, 1977] was used to measure the orientation of the facets on VL1 block from which the lighting and viewing angles were computed. Unit vectors for the normal poles to the two facets and for the incident solar rays, along with emission ray direction for VL1 block are shown projected onto a horizontal plane in Figure 6*a*. Facet 1 on VL1 block is tilted about 24° from the horizontal, whereas facet 2 is tilted about 58°. At the second landing site reflectance data for two facets of VL2 block were obtained from images acquired over a period of 45 Mars days. Again, stereo ranging was used to measure the orientation of the facets. The vector orientations for facets on VL2 block and the incident solar rays are shown in Figure 6*b*. Facet 1 on VL2 block is tilted about 32° from the horizontal, whereas facet 2 is tilted about 71°.

If the blocks had surfaces with homogeneous spectral properties, when seen at similar lighting and viewing geometries the reflectances should converge to similar values. In addition,

TABLE 1. Bidirectional Reflectance Estimates for Viking Lander Blocks and Soils

Location	Phase Angle	Reflectance			R/B Ratio	Curvature	Comments
		Blue	Green	Red			
Frame 11A147 (Lander 1, Camera 1)							
A1	90	0.13	0.18	0.29	2.23	1.16	VL1 block facet 1
A2	90	0.06	0.09	0.17	2.83	1.26	VL1 block facet 2
A3	87	0.07	0.12	0.20	2.86	0.97	block side
A4	81	0.10	0.16	0.32	3.20	1.25	block top
A5	75	0.12	0.19	0.39	3.25	1.30	block top
A6	87	0.08	0.12	0.18	2.25	1.00	block side
A7	76	0.07	0.11	0.27	3.86	1.56	soil
A8	77	0.08	0.13	0.30	3.75	1.42	soil
A9	65	0.07	0.11	0.22	3.14	1.27	soil
A10	77	0.07	0.12	0.22	3.14	1.07	block side
Frame 21A187 (Lander 2, Camera 1)							
B1	38	0.06	0.09	0.13	2.17	0.96	block side
B2	39	0.09	0.14	0.27	3.00	1.24	block side (on B1)
B3	58	0.06	0.09	0.17	2.83	1.26	block side
B4	62	0.05	0.09	0.20	4.00	1.23	block (same as C1)
B5	36	0.07	0.09	0.21	3.00	1.81	soil
B6	31	0.07	0.10	0.21	3.00	1.47	soil
B7	36	0.07	0.11	0.22	3.14	1.27	soil
B8	53	0.07	0.11	0.20	2.86	1.16	block side
B9	60	0.08	0.12	0.21	2.63	1.17	block side
Frame 22A190 (Lander 2, Camera 2)							
C1	56	0.05	0.10	0.21	4.20	1.05	block (same as B4)
C2	59	0.10	0.16	0.37	3.70	1.45	VL2 block facet 1
C3	62	0.09	0.12	0.19	2.11	1.19	VL2 block facet 2
C4	38	0.09	0.14	0.28	3.11	1.29	block top
C5	68	0.08	0.13	0.29	3.63	1.37	soil from drift
C6	64	0.06	0.10	0.22	3.67	1.32	soil
C7	73	0.06	0.09	0.20	3.33	1.48	soil
C8	54	0.07	0.11	0.20	2.86	1.16	soil
C9	49	0.07	0.11	0.24	3.43	1.39	soil
C10	67	0.07	0.12	0.27	3.86	1.31	possible duricrust
C11	73	0.06	0.09	0.21	3.50	1.55	soil
C12	73	0.07	0.11	0.22	3.14	1.27	block side

Reflectances have uncertainties of 10%. Locations are denoted in Figure 3.

the reflectances could be explained with similar values of B_0 and α. Plots of the reflectance data for the two blocks are shown in Figures 7*a* and 7*b*. The ordinate in Figure 7 is the term on the left side of (6) (referred to as the reflectance factor), while the abscissa is phase angle. Bidirectional reflectance estimates for the block facets, computed for incidence and phase angles of 20° and an emission angle of 0° using (5), are given in Table 2. This particular geometry was chosen because it is similar to the geometry used to measure the reflectance of laboratory samples discussed in the next section. VL1 block clearly has two spectrally distinct facets, since two distinctly different sets of B_0 and α are needed to explain the reflectances for the two facets. Facet 1 of VL1 block appears to be generally darker and less red than facet 2 when both facets are observed at similar geometries. For the VL2 block, a greater degree of scatter exists in the data, but two distinct trends are still evident. When the reflectance data for each facet of VL2 block are corrected to the same geometry, facet 2 is darker and less red than facet 1. In fact, facet 2 on VL2 block has among the lowest reflectances in the blue, green, and red channels for material at the landing sites.

The uncertainty in the data plotted in Figure 7 is related to uncertainties in calibrations, atmospheric opacity, orientation of the facets, and random noise in the data. The uncertainty in calibration is a constant factor for all data of a given facet since the data were obtained from a single camera. The data were also acquired over a relatively short period of time so that changes in calibration are negligible. Uncertainty due to random noise was minimized by averaging the response from several picture elements. On the other hand, uncertainty due to atmospheric opacity and orientation of the facets can vary between data points for a given facet because the data were acquired at different times and with different lighting conditions. The atmospheric opacity uncertainty is a function of the error in the measurement and of the solar incidence angle. For the data presented in Figure 7, this error averaged about 7%. We have empirically estimated how well the orientation of the facets are known by measuring the orientations of the facets on VL2 block several times using two separate sets of stereo images. The maximum differences between the measured poles to the facets was 65° in azimuth and 20° in elevation for facet 1 and 45° in azimuth and 5° in elevation for facet 2. These differences in pole orientations give rise to a variation in the cosine term of the reflectance factor that is a function of the lighting geometry. The average change of the cosine term for the lighting geometries used in this analysis was about 21%. The root-mean-square error from all sources of error is about 22%. Thus error bars in Figure 7 are ±22% of the reflectance factor value.

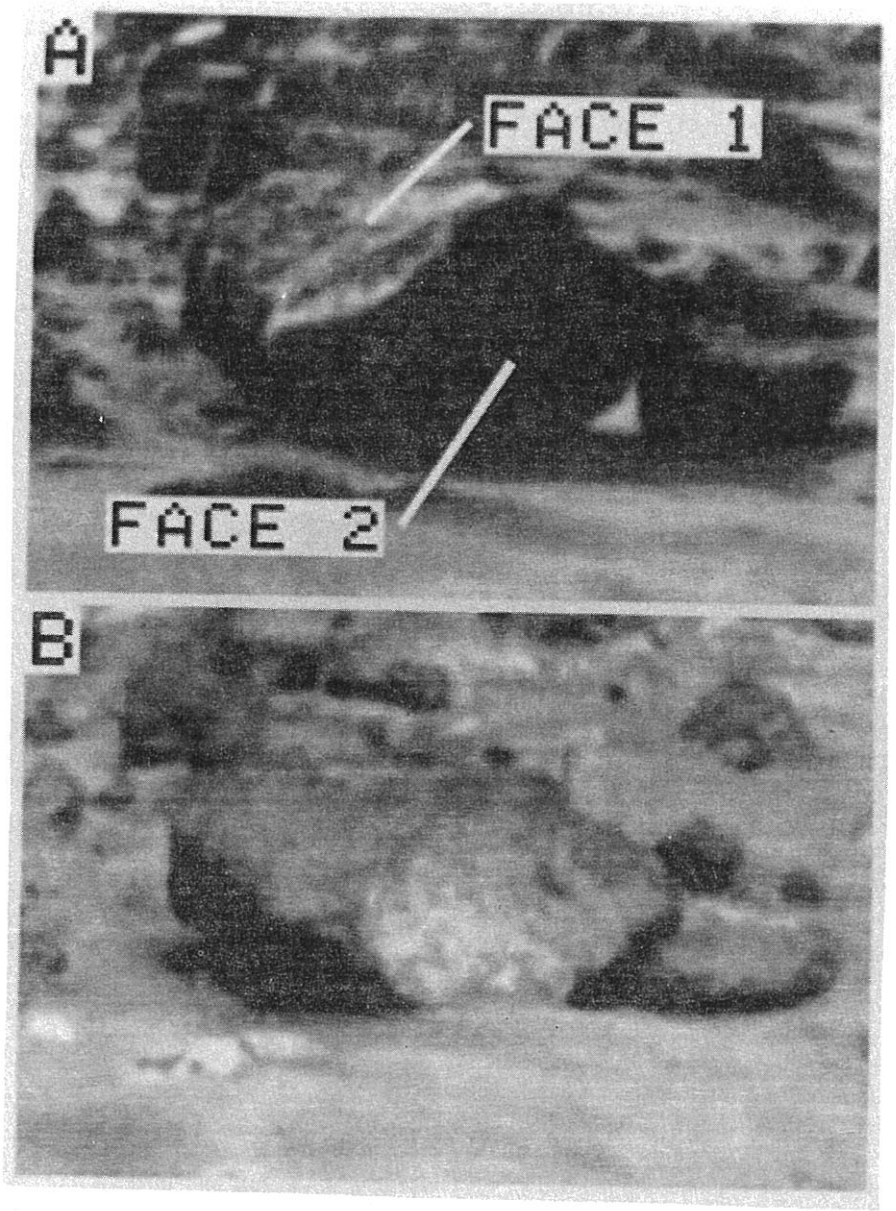

Fig 4. Two high resolution frames for the VL1 block (shown within the box in Figure 3*a*). These images were acquired with different lighting conditions. (*a*) VL1 image 11A097. Solar azimuth from north is 73° and elevation above the horizon is 27°. (*b*) VL1 image 11A127. Solar azimuth is 281° and elevation is 51°.

COMPARISON OF LANDER DATA WITH LABORATORY REFLECTANCE DATA

In this section mineralogical interpretations derived from the Lander blue, green, and red reflectance estimates are discussed. As previously stated, the blue, green, and red channels cover the wavelength range of about 0.4 to 0.74 μm. This wavelength range is particularly sensitive to the abundance, mineralogy, oxidation state, and degree of crystallinity of iron-bearing minerals. Crystalline ferric oxide minerals (e.g., hematite and geothite) exhibit strong absorptions in UV to visible wavelengths. For example, Figure 8*a* shows the spectrum of hematitically altered volcanic cinder that has significant spectral curvature between 0.5 and 0.6 μm. The absorptions are due to a charge transfer transition centered in the UV and to crystal field absorptions at about 0.45–0.53 and 0.62–0.64 μm [*Singer*, 1982; *Morris et al.*, 1985]. As a result, the reflectance of particulate ferric oxides is low (about 3%) from the UV to about 0.55 μm and then rises rapidly to a peak reflectance at about 0.75 μm, leading to a reflectance spectrum that is strongly curved in the visible [*Singer*, 1982; *Morris et al.*, 1985]. This spectral reflectance pattern is in contrast to the pattern observed for ferric iron-rich, amorphous materials such as some palagonites (Figure 8*a*). The spectrum of this palagonite is characterized by a straighter, relatively featureless rise in reflectance from the UV to about 0.8 μm that is caused by a lack of crystal field absorptions due to the absence of a well-defined crystalline structure [*Singer*, 1982]. The spectral reflectance of mafic rocks containing ferrous iron-bearing silicates is generally lower and less steeply sloped in the visible than ferric-iron phases (Figure 8*a*) [*Hunt et al.*, 1974; *Adams*, 1975]. Mafic rocks also tend to have low reflectances in the near-infrared region because of absorptions by optically opaque phases and by electronic absorptions due to ferrous bearing silicates [*Hunt et al.*, 1974].

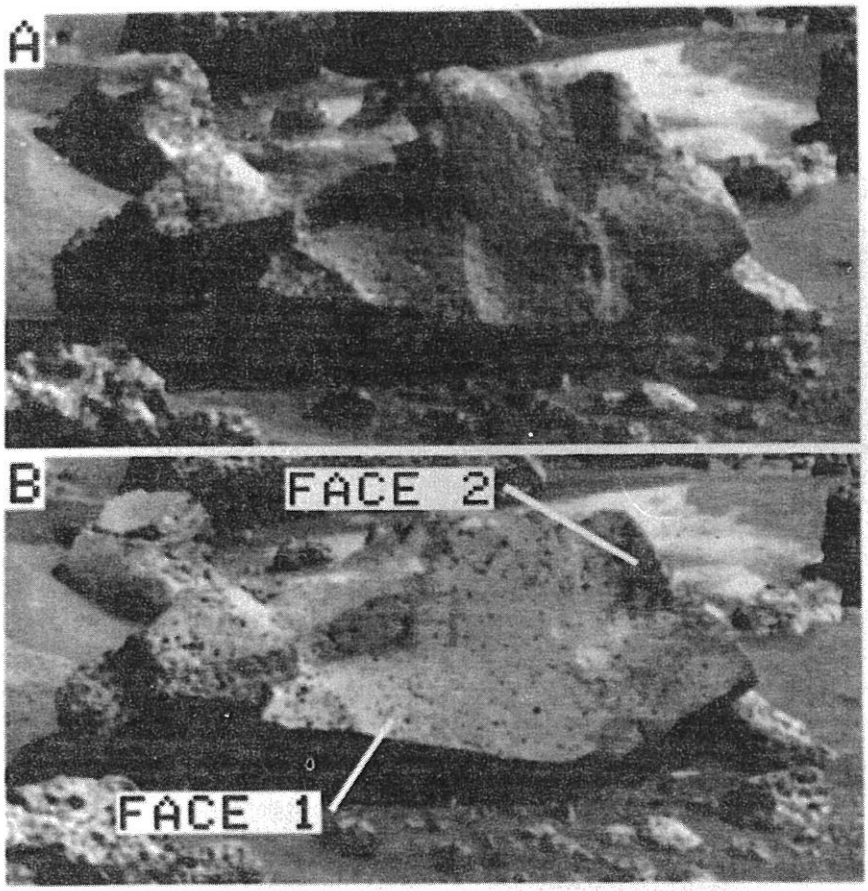

Fig. 5. Two high resolution frames for the VL2 block (shown within the box in Figure 3*c*). These images were acquired with different lighting conditions. (*a*) VL2 image 22A137. Solar azimuth is 117° and elevation is 47°. (*b*) VL2 image 22A252. Solar azimuth is 176° and elevation is 60°.

With this general background of relevant spectral properties, we now address the Lander reflectance data. The Lander data listed in Table 1 were compared to laboratory spectra of selected materials and earth-based telescopic spectra of Mars. First, both the laboratory and telescopic data were resampled to the Lander color bandpasses (Figure 8*b*). As previously discussed, this step is essential because of the broad widths and irregular shapes of the Lander channels. Laboratory analogs used for this analysis were chosen primarily for their compositional and spectral relevance to Mars, based on the interpretation of, for example, Viking Lander chemical measurements and earth-based telescopic reflectance spectra. Samples included the ferric oxides hematite, goethite, and limonite, two Hawaiian palagonitic soils, hematitically altered volcanic cinders, and seven mafic igneous rocks (fresh and weathered surfaces of each). Four telescopic spectra were chosen as representative data in the spectral region of interest, including a bright region and a dark region observation from both the 1969 [*McCord and Westphal*, 1971] and 1973 [*McCord et al.*, 1977] oppositions. Because these telescopic spectra are relative rather than absolute reflectance, they required scaling by a multiplicative constant to allow comparisons to Lander data. This scaling does not affect color and slope information, only overall reflectance.

The comparisons of the Lander reflectance data to laboratory spectral data was primarily based on spectral shape. The blue, green, and red reflectances can be used to characterize spectral shape in terms of slope and spectral curvature. A simple measure of the curvature in Lander reflectance spectra can be defined as follows

$$C = \frac{(\rho_r \rho_b)}{\rho_g^2} \quad (7$$

where C is the measure of curvature and ρ_b, ρ_g, and ρ_r ar the reflectances determined for the blue, green, and red channels respectively. The curvature measure can be thought of as a rati of red/green and green/blue ratios. We found that this curvatur parameter is related to ferric oxide mineral type as well as degre of crystallinity in laboratory samples. Larger values of C would for example, be consistent with greater degrees of ferric iro crystallinity because the green channel is sensitive to the dept of the ferric iron absorption near 0.45–0.54 μm. This measur is also very sensitive to the spectral difference between miner phases such as hematite and goethite. In addition, we use th ratio of the red and blue reflectances as a measure of slop of the spectra. The red/blue ratio will generally increase as th

TABLE 2. Bidirectional Reflectance Estimates for Blocks

Location	Reflectance		
	Blue	Green	Red
VL1 block facet 1	0.09	0.13	0.23
VL1 block facet 2	0.13	0.21	0.43
VL2 block facet 1	0.09	0.16	0.36
VL2 block facet 2	0.06	0.09	0.15

Corrected to 20° incidence and phase angles, and 0° emission angle

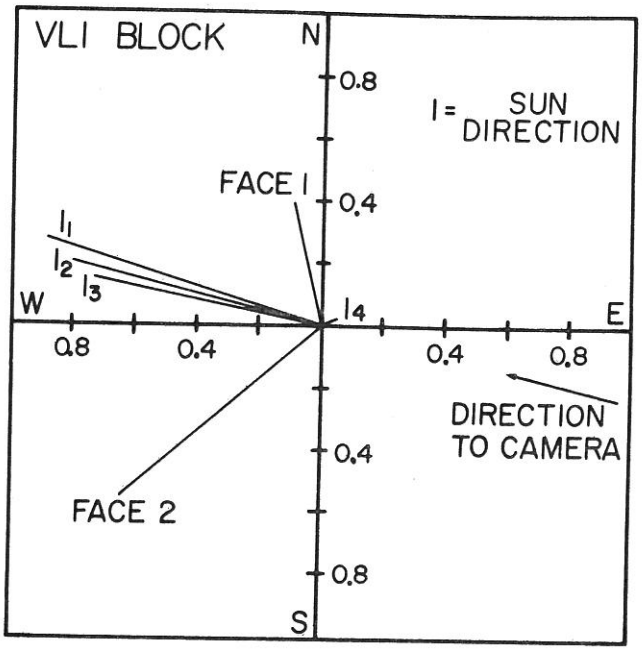

Fig. 6a

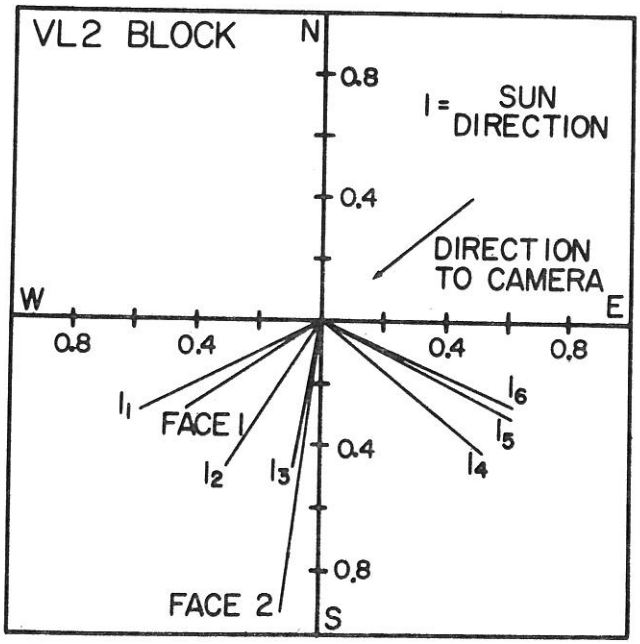

Fig. 6b

Fig. 6. These plots are horizontal planes showing the orientation of the facets of VL1 and VL2 blocks and the lighting and viewing geometry for images used to study the photometry of the facets. The vertical axis of the diagram is aligned in a north-south direction. Each facet orientation is shown as the projection of the unit vector normal to the plane of the facet. Sun direction and facet orientations are also represented as projections of unit vectors onto the horizontal plane. The longer the facet vector, the more vertical the facet is oriented. Longer sun direction vectors mean smaller solar elevation angles. Sun vectors are numbered according to increasing phase angle (see Figure 7) for each block. (*a*) VL1 block. (*b*) VL2 block.

degree of oxidation of iron bearing materials increases [*Evans et al.*, 1981; *McCord et al.*, 1982]. Values of curvature and slope for the 31 samples of soil and blocks at the landing sites are given in Table 1.

The block surface with the lowest overall reflectance and slope is facet 2 of VL2 block (sample C3 from Table 1). The reflectance of C3 is a good match to unoxidized Mauna Kea basaltic andesite (Mugearite) naturally coated with about 30 μm of exogenetically derived palagonite, and also to the telescopic dark regions (Figure 9*a*) [*Singer*, 1980]. This inference is corroborated by an examination of images from the three Lander Camera infrared channels. The brightness of the dark facet on VL2 block (C3) in infrared images is lower than surrounding soil by a factor of 2, consistent with greater optical influence from underlying mafic materials on the dark facet [*Dale-Bannister et al.*, 1985]. Soil sample C8 (Table 1) is a good match in slope and amount of spectral curvature to both the telescopic bright regions and a Mauna Kea palagonite [VOLO2A, *Singer*, 1982; and H-34, *Evans and Adams*, 1979] (Figure 9*b*). This soil sample has the lowest slope and least curved spectra for all of the soils sampled. Most block surfaces have slopes intermediate between those for samples C3 and C8, although they vary significantly in overall reflectance. The shapes of the spectra for these blocks are similar to the spectra of telescopic bright regions and the palagonite

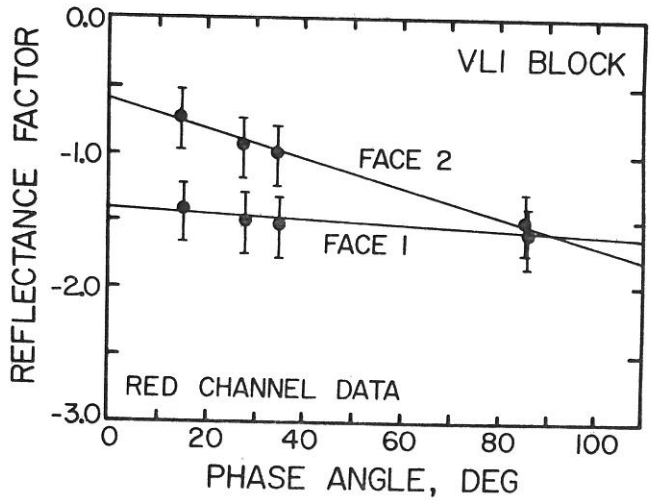

Fig. 7a

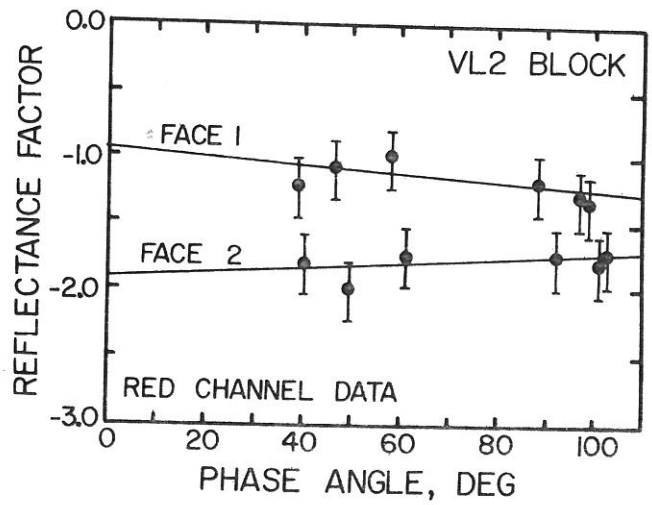

Fig. 7b

Fig. 7. Hapke-Irvine plots for VL1 and VL2 blocks. The reflectance factor is the term on the left side of (6). The solid lines are the least-square fits to the data. The relative error in the data points is 22% as discussed in the text. Data for the red channel are shown. (*a*) VL1 block. (*b*) VL2 block.

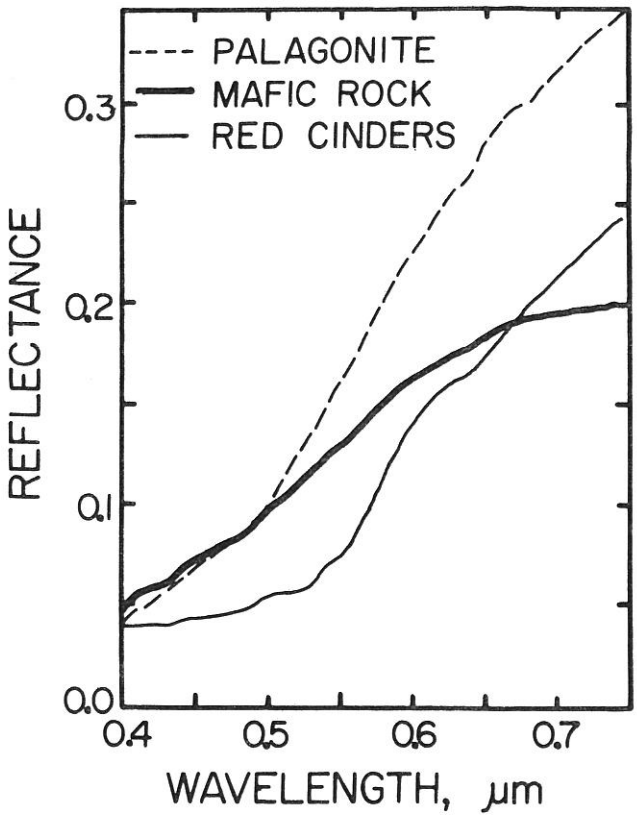

Fig. 8*a*

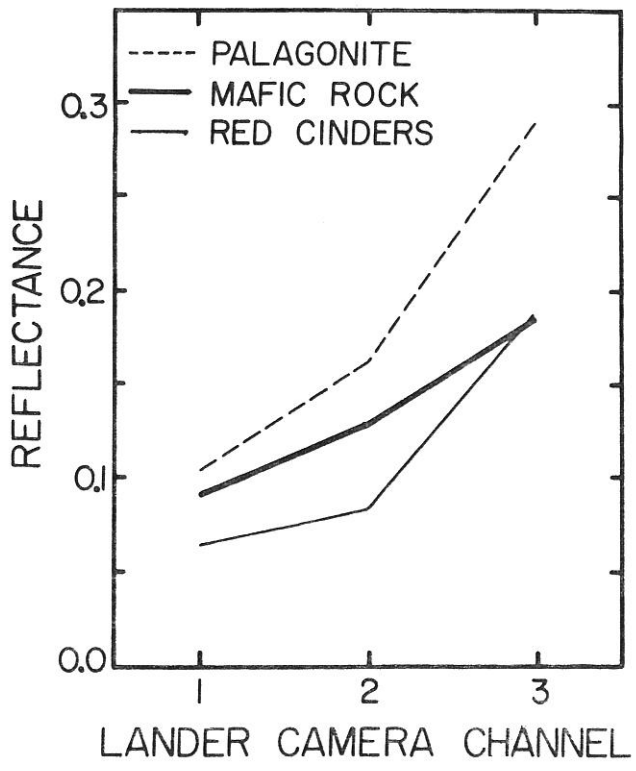

Fig. 8*b*

Fig. 8. Laboratory reflectance data for a palagonite sample, a thinly coated mafic rock, and a sample of hematitically altered volcanic cinder are shown for the wavelengths covered by the Viking Lander color channels. (*a*) Original laboratory data. (*b*) Resampled three point spectra. Channel 1 refers to the Lander Camera blue channel, 2 to the green channel, and 3 to the red channel.

discussed above (VOLO2A). Thus the spectral signatures of these blocks are consistent with coatings of palagonite material, varying from being thin, semitransparent to being optically thick, over dark unoxidized rock.

There is a limited exposure of relatively dark, red soil at the Lander 2 site (B5) that has a significantly larger spectral curvature than the other block and soil samples. Reflectance data for this soil are consistent with the degraded spectrum of red, hematitically altered volcanic cinder from Mauna Kea (Figure 10), but not for pure hematite or other iron oxides. This small exposure may be a hematitically altered soil, grading into the more common soil that surrounds it. This is an important observation because hematite forms under distinctly different conditions than thought for the more common martian soils and dust [*Soderblom et al.*, 1978; *McCord et al.*, 1982; *Singer*, 1982; *Morris and Lauer*, 1986].

The vast majority of soils sampled at both landing sites as well as a few block exposures are not consistent with any of the laboratory or telescopic spectra used in this study. Unfortunately, no telescopic spectra over the landing sites are available. Soil samples for which no laboratory analog was found tend to have higher values of spectral slope and have curvatures that are intermediate between C8 and B5. A few blocks, such as C2, also have reflectance properties similar to these soil samples and are interpreted to have optically thick coatings of this soil type. As discussed, spectral curvature in laboratory samples is related to ferric oxide mineral type as well as degree of crystallinity. The larger curvature values would be consistent with greater degrees of ferric iron crystallinity. The differences in spectral shape (slope and curvature) seen for soils and blocks at the landing sites could be due to variations in the degree of oxidation and crystallinity of iron-bearing materials, to variations in incidence, emission, and phase angles, or to variations in particular size. Calibration uncertainties do not appear to account for the variations in spectral shape because there is no correlation between the camera that acquired the data and spectral shape. Changes in slope with phase angle for small soil patches at Viking Lander 1 [*Guinness*, 1981] are nearly an order of magnitude smaller than observed for soils sampled here. This result, combined with the result that spectrally distinct facets exist on individual blocks, suggests that variations in lighting and viewing geometry do not explain all of the observed variations in spectral shape.

The effects of varying particle size on reflectance should be considered in two ways: (1) soils with one lithology that have different reflectance properties, depending on grain size, and (2) soils that may compositionally fractionate as a function of particle size. The particle size effects that are usually studied in the laboratory and applied to remote-sensing analyses concern the spectral behavior of a single lithology. For most monolithologic materials, with low to moderate absorption coefficients, decreasing the particle size increases overall reflectance and slightly increases the spectral slope. Significant spectral shape changes are not observed [*Adams and Filice*, 1967]. *Evans et al.* [1981] and *McCord et al.* [1982] demonstrated that these effects are not large enough to account for most of the reflectance variations seen in Viking Orbiter multispectral data. The same conclusion would appear to be true for Viking Lander reflectance data. For soils on earth where the lithologies change with grain size, the coarse-grained fractions of soils tend to be relatively enriched in unaltered material, while the fine-grained fractions are enriched in weathered materials. Because these two size fractions are mineralogically different and usually

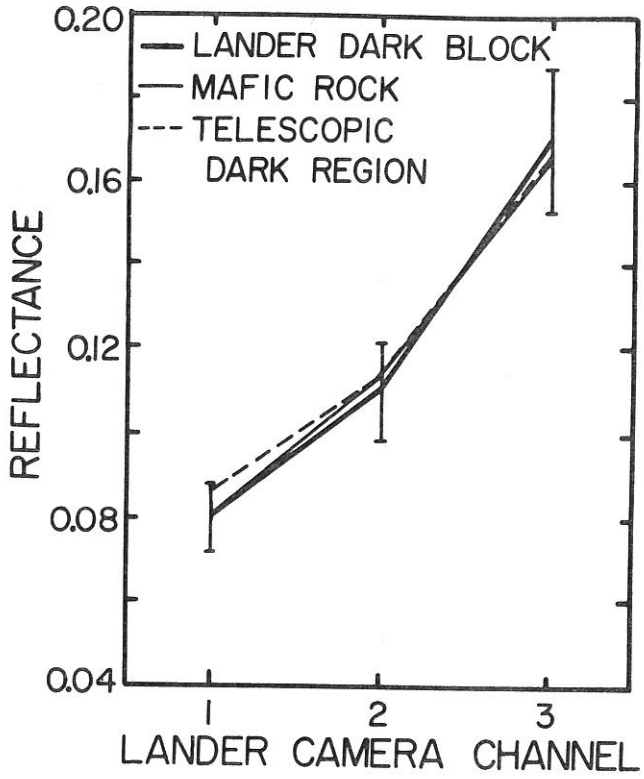

Fig. 9*a*

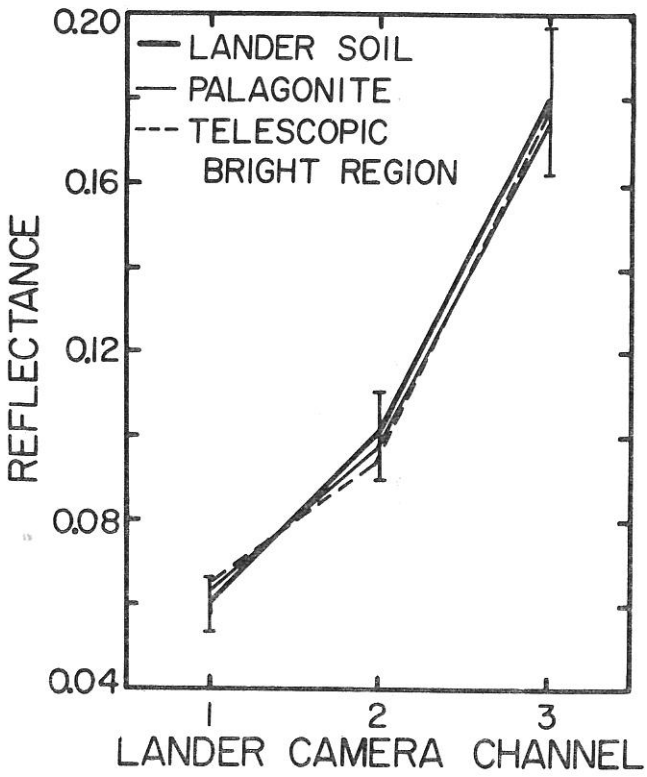

Fig. 9*b*

Fig. 9. Reflectance versus channel number for the dark block sample C3 and soil sample C8. Channel 1 refers to the blue channel, 2 to green, and 3 to red. The error bars represent 10% uncertainty in reflectance for the Lander data. The best matches to these examples from resampled laboratory and telescopic reflectance data are also plotted. The laboratory and telescopic spectra were scaled by a constant to overlie the Lander data. The rescaling, however, does not affect spectral shape, only overall reflectance. (*a*) Lander sample C3 with unoxidized basalt and telescopic dark region spectra. (*b*) Lander sample C8 with palagonite and telescopic bright region spectra.

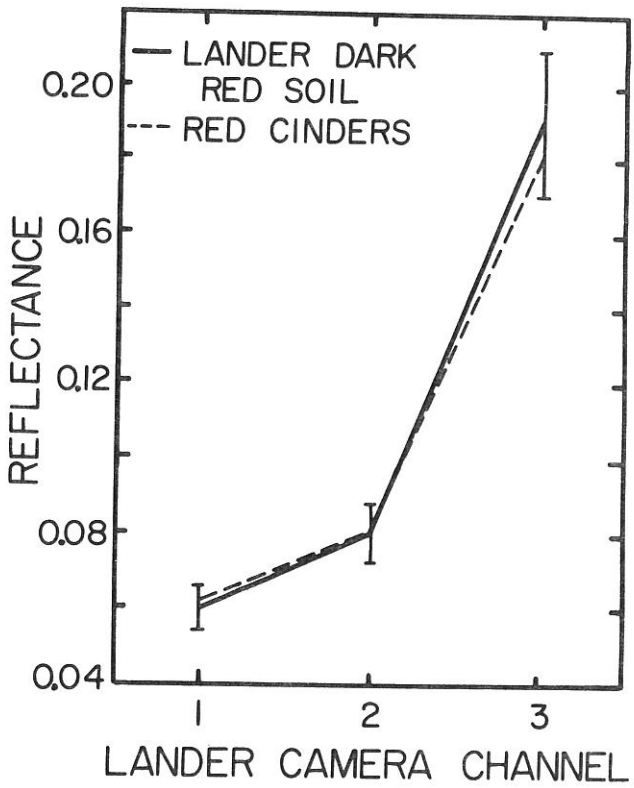

Fig. 10. Reflectance versus channel number for Lander soil (B5) with the largest curvature value. Channel 1 refers to the blue channel, 2 to green, and 3 to red. The error bars represent 10% uncertainty in reflectance for the Lander data. The resampled reflectance spectrum of red, hematitically altered volcanic cinder is also plotted. The laboratory spectrum was scaled by a constant to overlie the Lander data. The rescaling, however, does not affect the spectral shape, only overall reflectance.

have different spectral properties, sorting mechanisms on earth typically do produce significant changes in observed reflectance.

We conclude, based on comparison to laboratory spectra and on the above discussion, that composition (i.e., degree of oxidation, mineralogy, and crystallinity) varies among the different soil samples. From the blue, green, and red reflectance data alone, we cannot test whether these variations are due to compositions that vary with particle size. However, other Mars data indicate that composition is correlated with particle size. For example, the fine-grained dust deposited after the 1977 global dust storm was similar in color to the brightest, reddest soil at the landing sites [*Guinness et al.*, 1979]. On a regional scale high thermal inertia regions (i.e., coarser material) have lower albedos than low thermal inertia (i.e., finer material) regions [*Kieffer et al.*, 1977]. In addition, as noted by several researchers, sand-sized dune material on Mars tends to be darker and grayer than surrounding finer material [*Singer et al.*, 1984; *Thomas*, 1984].

DISCUSSION

Reflectances derived for the soils and blocks at the two Viking Landing sites are consistent with the conclusion that blocks seen at both sites are mafic rocks coated to varying thicknesses with somewhat amorphous, oxidized material. More rigorous determination of substrate rock composition (e.g., ultramafic, basalt, or basaltic andesite) requires complete spectral data in the near-infrared region. Palagonites, or more properly, ferric iron-rich, somewhat amorphous weathering products, are

reasonable analogs for limited exposures of soils and block coatings. Major questions still remain as to how weathering has occurred on Mars. *Baird and Clark* [1981] make compelling arguments that soils are derived from mafic to ultramafic source blocks in some isochemical process. Palagonitization of basaltic magmas and basaltic glass has also been proposed as an important mechanism [*Soderblom and Wenner*, 1978; *Allen et al.*, 1981]. Palagonite is a broad term, encompassing a variety of related materials with different origins and spectral properties, and only specific palagonites are reasonable spectral analogs to Mars [*Singer*, 1982]. However, all palagonites are relatively low-temperature alteration products of mafic volcanic glass.

The spectral shape of most observed soils as opposed to blocks implies that soils at the landing sites have not been produced by local weathering of blocks, since the soil reflectance signatures are distinctly different from most blocks. It is possible that material weathered from blocks is intimately mixed with a soil end member not exposed at the landing site that has greater slope and curvature than palagonite-like coatings on blocks. Even if such mixing occurs, it implies that soils at the landing sites are not predominantly derived from local weathering of blocks. A more plausible scenario is one where soils are created globally by a number of processes that operated at higher rates earlier in geologic time. The materials would then be transported and would accumulate at a variety of locations. Once deposited, further erosion would sort the material and evaporation of fluids would lead to generation of duricrust. At least at the landing sites, blocks would have been steadily added to the site by impact events and exposed to slow, perhaps steady state weathering generating only a small amount of soil. This scenario implies that the bulk of the soil at the sites carry little information about the local geology.

SUMMARY

Bidirectional reflectances for the blue, green, and red channels were determined for 31 soil and block exposures imaged by the Viking Lander Cameras on Mars. The reflectances were calibrated to within 10% uncertainties. Preflight calibrations were tested by analyses of the brightness values obtained from sunlit and shadowed gray patches mounted on the Landers, which have well-defined Lambertian scattering characteristics. Reflectances of soils and blocks were corrected for atmospheric attenuation by using optical depth measurements obtained by the Lander Cameras and for skylight illumination by subtracting the brightness values for adjacent shadowed areas. Reflectances of two facets on each of two large blocks were computed for a common geometry by determining facet orientations from high resolution Lander stereo images and by fitting the Hapke-Irvine photometric function to reflectance data acquired at several different geometries. Results indicate that individual facets on the same block have different spectral reflectance properties.

The variations in bidirectional reflectance in the visible and relative brightness in the infrared can best be explained by varying degrees of oxidation and ferric iron crystallinity. The darkest, grayest block surfaces are consistent with laboratory reflectance spectra of mafic rocks, thinly coated with ferric iron-rich palagonite. Such a result is consistent with the low relative reflectance for the dark facets determined from images acquired with the Lander Camera infrared channels. Most block surfaces are consistent with thin to optically thick covers of palagonitic material. Limited exposures of soil have blue, green, and red reflectances that are similar to palagonitic material. One soil exposure has a spectral shape that is similar to a sample of hematitically altered volcanic cinder. The bulk of the soils sampled and a few block surfaces have spectra with steeper slopes and larger curvatures than the palagonite analog. In particular, one reasonable interpretation is that the most commonly sampled soil exposed at the landing sites may have a greater degree of ferric iron crystallinity than the palagonite analog. These soils could also be an intimate mixture of palagonite material and other materials not seen in end-member form. If intimate mixing occurs, however, these other materials would need an even greater slope and curvature than the observed soils, and presumably be even more different from material seen on block surfaces in terms of the degree of ferric iron crystallinity. Finally, it seems improbable that the bulk of soils could have been derived from weathering of local blocks since most soils have distinctly different blue, green, and red reflectances from most block surfaces.

Acknowledgments. This work was carried out as part of the NASA Planetary Geology Program Grant NSG-7087 to Washington University and Grant NSG-7590 to the University of Hawaii. H. Kieffer and M. Smith provided helpful reviews of the manuscript.

REFERENCES

Adams, J. B., Interpretation of visible and near-infrared diffuse reflectance spectra of pyroxenes and other rock-forming minerals, in *Infrared and Raman Spectroscopy of Lunar and Terrestrial Minerals*, edited by C. Kerr, pp. 91–116, Academic, New York, 1975.

Adams, J. B., and A. L. Filice, Spectral reflectance 0.4 to 2.0 microns of silicate rock powders, *J. Geophys. Res., 72*, 5705–5715, 1967.

Adams, J. B., M. O. Smith, and P. E. Johnson, Spectral mixture modeling: A new analysis of rock and soil types at the Viking Lander 1 site, *J. Geophys. Res., 91*, 8098–8112, 1986.

Allen, C. C., J. L. Gooding, M. Jercinovic, and K. Keil, Altered basaltic glass: A terrestrial analog to the soil of Mars, *Icarus, 45*, 347–369, 1981.

Arvidson, R. E., E. A. Guinness, H. J. Moore, J. Tillman, and S. D. Wall, Three Mars years: Viking Lander 1 imaging observations, *Science, 222*, 463–468, 1983.

Baird, A. K., and B. C. Clark, On the original igneous source of martian fines, *Icarus, 45*, 113–123, 1981.

Binder, A. B., R. E. Arvidson, E. A. Guinness, K. L. Jones, E. C. Morris, T. A. Mutch, D. C. Pieri, and C. Sagan, The geology of the Viking Lander 1 site, *J. Geophys. Res., 82*, 4439–4451, 1977.

Dale-Bannister, M., R. Arvidson, R. Singer, and E. Bruckenthal, The search for igneous minerals at the Viking Lander sites (abstract), in *Lunar and Planetary Science XVI*, pp. 161–162, Lunar and Planetary Institute, Houston, 1985.

Evans, D. L., and J. B. Adams, Comparison of Viking Lander multispectral images and laboratory reflectance spectra of terrestrial samples, *Proc. Lunar Planet. Sci. Conf. 10th*, 1829–1834, 1979.

Evans, D. L., and J. B. Adams, Amorphous gels as possible analogs to martian weathering products, *Proc. Lunar Planet. Sci. Conf. 11th*, 757–763, 1980.

Evans, D. L., T. G. Farr, and J. B. Adams, Spectral reflectance of weathered terrestrial and martian surfaces, *Proc. Lunar Planet. Sci. 12B*, 1473–1479, 1981.

Gradie, J., J. Veverka, and B. Buratti, The effects of scattering geometry on the spectrophotometric properties of powdered material, *Proc. Lunar Planet. Sci. Conf. 11th*, 799–815, 1980.

Guinness, E. A., Spectral properties (0.40 to 0.75 microns) of soils exposed at the Viking 1 Landing site, *J. Geophys. Res., 86*, 7983–7992, 1981.

Guinness, E. A., R. E. Arvidson, D. C. Gehret, and L. K. Bolef, Color changes at the Viking landing sites over the course of a Mars year, *J. Geophys. Res., 84*, 8355–8364, 1979.

Hapke, B., Bi-directional reflectance spectroscopy, 1, Theory, *J. Geophys. Res., 86*, 3039–3054, 1981.

Huck, F. O., E. E. Burcher, E. J. Taylor, and S. D. Wall, Radiometric performance of the Viking Mars Lander Cameras, *NASA TM X-72692*, 1975.

Huck, F. O., D. J. Jobson, S. K. Park, S. D. Wall, R. E. Arvidson,

W. R. Patterson, and W. D. Benton, Spectrophotometric and color estimates of the Viking landing sites, *J. Geophys. Res., 82*, 4401–4411, 1977.

Hunt, G. R., J. W. Salisbury, and C. J. Lenhoff, Visible and near infrared spectra of minerals and rocks: IX. Basic and ultrabasic igneous rocks, *Mod. Geol., 5*, 15–22, 1974.

Kieffer, H. H., T. Z. Martin, A. R. Peterfreund, and B. M. Jakosky, Thermal and albedo mapping of Mars during the Viking Primary Mission, *J. Geophys. Res., 82*, 4249–4291, 1977.

Liebes, S., Jr., and A. A. Schwartz, Viking 1975 Mars Lander interactive computerized video stereophotogrammetry, *J. Geophys. Res., 82*, 4421–4429, 1977.

McCord, T. B., and J. A. Westphal, Mars: Narrow-band photometry, from 0.3 to 2.5 microns, of surface regions during the 1969 apparition, *Astrophys. J., 168*, 141–153, 1971.

McCord, T. B., R. L. Huguenin, and G. L. Johnson, Photometric imaging of Mars during the 1973 opposition, *Icarus, 31*, 293–314, 1977.

McCord, T. B., R. B. Singer, B. R. Hawke, J. B. Adams, D. L. Evans, J. W. Head, P. J. Mouginis-Mark, C. M. Pieters, R. L. Huguenin, and S. H. Zisk, Mars: Definition and characterization of global surface units with emphasis on composition, *J. Geophys. Res., 87*, 10,129–10,148, 1982.

Morris, R. V., and H. V. Lauer, Evidence for hematite on Mars: Spectral properties of ferric iron phases in annealed, Al-rich precipitates of Fe-Al sulfate salt solutions (abstract), in *Lunar and Planetary Science, XVII*, pp. 573–574, Lunar and Planetary Institute, Houston, 1986.

Morris, R. V., H. V. Lauer, C. A. Lawson, E. K. Gibson, G. A. Nace, and C. Stewart, Spectral and other physiochemical properties of submicron powders of hematite (α-Fe_2O_3), maghemite (γ-Fe_2O_3), magnetite (Fe_3O_4), goethite (α-FeOOH), and leipocrocite (γ-FeOOH), *J. Geophys. Res., 90*, 3126–3144, 1985.

Mutch, T. A., R. E. Arvidson, A. B. Binder, E. A. Guinness, and E. C. Morris, The geology of the Viking Lander 2 site, *J. Geophys. Res., 82*, 4452–4467, 1977.

Patterson, W. R., F. O. Huck, S. D. Wall, and M. R. Wolf, Calibration and performance of the Viking Lander Cameras, *J. Geophys. Res., 82*, 4391–4400, 1977.

Pollack, J. B., D. Colburn, R. Kahn, J. Hunter, W. VanCamp, C. E. Carlston, and M. R. Wolf, Properties of Aerosols in the martian atmosphere as inferred from Viking Lander imaging data, *J. Geophys. Res., 82*, 4479–4496, 1977.

Pollack, J. B., D. G. Colburn, F. M. Flasar, R. Kahn, C. E. Carlston, and D. Pidek, Properties and effects of dust particles suspended in the martian atmosphere, *J. Geophys. Res., 84*, 2929–2945, 1979.

Sharp, R. P., and M. C. Malin, Surface geology from Viking Landers on Mars: A second look, *Geol. Soc. Am. Bull., 95*, 1398–1412, 1984.

Singer, R. B., The dark materials on Mars: I. New information from reflectance spectroscopy on the extent and mode of oxidation (abstract), in *Lunar and Planetary Science XI*, pp. 1045–1047, Lunar and Planetary Institute, Houston, 1980.

Singer, R. B., Spectral evidence for the mineralogy of high-albedo soils and dust on mars, *J. Geophys. Res., 87*, 10,159–10,168, 1982.

Singer, R. B., and E. L. Strickland, Spectral variety of martian surface materials: Comparison of earth-based and Viking Lander data (abstract), in *Lunar and Planetary Science XII*, pp. 999–1001, Lunar and Planetary Institute, Houston, 1981.

Singer, R. B., E. Cloutis, T. L. Roush, P. J. Mouginis-Mark, B. R. Hawke, and P. R. Christensen, Multispectral analysis of the Kasei Vallis—Lunae Planum region on Mars (abstract), in *Lunar and Planetary Science XV*, pp. 794–795, Lunar and Planetary Institute, Houston, 1984.

Soderblom, L. A., and D. B. Wenner, Possible fossil H_2O liquid-ice interfaces in the martian crust, *Icarus, 34*, 622–637, 1978.

Soderblom, L. A., K. Edwards, E. M. Eliason, E. M. Sanchez, and M. P. Charette, Global color variations on the martian surface, *Icarus, 34*, 446–464, 1978.

Strickland, E. L., III, Soil stratigraphy and rock coatings observed in color enhanced Viking Lander images, *Proc. Lunar Planet. Sci. Conf. 10th*, 3055–3077, 1979.

Thomas, P., Martian intercrater splotches: Occurrence, morphology, and colors, *Icarus, 57*, 205–227, 1984.

Wall, S. D., E. E. Burcher, and D. J. Jobson, Reflectance characteristics of the Viking Lander Camera reference test charts, *NASA TM X-72762*, 1975.

E. A. Guinness, R. E. Arvidson, and M. A. Dale-Bannister, McDonnell Center for the Space Sciences, Department of Earth and Planetary Sciences, Washington University, St. Louis, MO 63130.

R. B. Singer and E. A. Bruckenthal, Planetary Geosciences Division, Hawaii Institute of Geophysics, University of Hawaii, Honolulu, HI 96822.

(Received April 28, 1986;
revised September 16, 1986;
accepted October 24, 1986.)